Journal of Thermal Analysis and Calorimetry, Vol. 86 (2006) 1, 187–194

ON THE PREPARATION OF SYNTHETIC CARBON ADSORBENTS USING THE SULFONATED ION EXCHANGE RESIN DUOLITE C-20

J. Skubiszewska-Zięba[1*], *R. Leboda*[1], *B. Charmas*[1], *W. Grzegorczyk*[1] *and R. Szmigielski*[2]

[1]Faculty of Chemistry, Maria Curie-Skłodowska University, M. C. Skłodowska 3 Sq., 20-031 Lublin, Poland
[2]Military Institute of Chemistry and Radiometry, 00-910 Warsaw, Poland

Thermal analysis was used to study thermal behavior of the sulfonated ion exchange resin Duolite C20 in the hydrogen, sodium and calcium forms. The aim of this paper was to prepare spherical carbon adsorbents. SEM and AFM microscopic methods have been applied to describe their surface characteristics. It was stated that structural parameters of prepared active carbons depend on the kind of cation present in the resin. The use of calcium form of Duolite C20 as the initial polymer precursor allowed to obtain the active carbon with better yield and better developed pore structure compared with other forms of this ion exchanger.

Keywords: *AFM, Duolite C20, ion-exchanger, pyrolysis, SEM, thermal analysis*

Introduction

Synthetic active carbons derived from certain kinds of porous copolymers or ion-exchange resins provide a new type of carbon adsorbents [1]. Such synthetic active carbons have some advantages over other types of carbon adsorbents because of a set of properties, characteristic of this type of carbon, such as high mechanical strength and sorption capacity as well as high purity and regular spherical shape of the granules. Recently there has been noticed a growing interest in the production of adsorbents from phenol-formaldehyde resins [2–4] and sulfonated polystyrene- and divinylbenzene-based resins [5–10]. However, use of waste ion-exchange resins for this purpose may be of very large economical and ecological advantage [5, 8, 10].

Ion-exchange resins, mostly polystyrene resins, are widely used for deionization of boiler water, water in nuclear power plants, for sewage treatment, for metal separation from aqueous solutions, etc. Dubois *et al.* [8] state that the embedded spent resins may undergo radiolytic or chemical degradation, which may result in the emission of hazardous species into the environment. However, Bratek *et al.* [5] point to the experiments described in literature in which raw polymers have mostly been used as initial materials for preparation of synthetic carbons. The properties of an activated carbon or an activated carbon fibre are conditioned both by the nature of the precursor and by the activating agents and the conditions of the pyrolysis and activation processes. The knowledge of the phenomena involved in the thermal degradation of the raw material can contribute to the right choice of the pyrolysis conditions. Recently Villar-Rodil *et al.* [11] studied the possibility of preparation of activated carbon fibres with narrow pore size distribution on the basis of polyamide polymer (Nomex). The studies of thermal behaviour of many kinds of synthetic polymers [12–17] are the important problems also from the point of view of their further application as carbon materials. It seems very interesting to study the behaviour of ion-exchange resins containing metal ions that can catalyse some thermal decomposition processes and activation of obtained carbonizates. Paper [5] points to also to the lack of the systematic studies showing the effect of condition of resin carbonization and activation on the properties and structure of the obtained synthetic carbons. Therefore this paper presents the results of studies on the effect of form (type of embedded cation) of the ion exchanger Duolite C20 on pyrolysis course, properties of obtained carbonizates as well as porous structure of synthetic carbon adsorbents prepared on their basis (through their activation). The hydrogen from of Duolite C20 (manufactured by Rohm and Haas) was investigated in detail by Dubois *et al.* [8] in order to identify volatile substances formed due to thermal resin degradation (in air and nitrogen atmosphere) in the temperature range 20–1000°C. The paper provides much valuable information about behaviour of strong-acid-cation exchangers and strong-base-anion exchangers typically used in nuclear power plants at various temperatures.

Experimental

Materials

The starting material in the investigations was the commercial ion-exchange resin Duolite C20 in the so-

* Author for correspondence: jskubisz@o2.pl

1388–6150/$20.00

Akadémiai Kiadó, Budapest, Hungary
Springer, Dordrecht, The Netherlands

dium form containing the functional sulfone groups, produced by Vitry Chauny (France). It is a strong acid-cation exchanger styrene (92%) divinylbenzene (8%) copolymer. Its cationic capacity is 5 meq g^{-1} or 2.2 meq mL^{-1}. It means that in starting material the concentration of sodium is about 11 mass/mass%. It is known [18, 19], that calcium is a very effective catalyst of carbon material gasification. It allows obtain active carbons with good developed micro-, and mesoporous structure. So the initial sodium (D–Na), and prepared hydrogen (D–H) and calcium (D–Ca) forms were pyrolised. The grain size used in preparation was 0.3–1.2 mm. The symbols of pyrolysis products (the obtained carbon materials) used further are given in brackets.

The hydrogen form was prepared in the standard way by swelling the commercial resin in the distilled water (6 h, 80°C), washing with 2 M hydrochloric acid solution and next by washing the acid with distilled water from the ion exchanger surface and drying at 100°C. The calcium form was prepared in a similar way by treating the swollen ion exchanger in the hydrogen form with a suitable amount of 0.1 M aqueous calcium acetate solution.

Calcium concentration in solutions before and after ion exchange was controlled using atomic absorption spectroscopy (AASA) by means of the apparatus Spectr AA 880 produced by Varian (Australia). On the basis of this data it was determined that calcium concentration in D–Ca form of resin was 2.5 meq g^{-1}, i.e., 5 mass/mass%. It means that about 50% ion-exchanging capacity was used.

Carbonization

Pyrolysis process of the starting Duolite C20 samples was studied with the linear increment of temperature with a rate 5°C min^{-1} in the deoxidized argon atmosphere using the high-sensitive derivatograph produced by MOM Hungary (Derivatograph-PC, Paulik–Paulik–Erdey system).

Carbonization of the Duolite C20 samples was carried out in the fluidal quartz reactor. Conditions: heating with the rate 5°C min^{-1} up to 800°C, then heating at 800°C for 0.5 h. The atmosphere: hydrogen+deoxidized nitrogen (1:1), the flow rate through the reactor – 200 mL min^{-1} of each gas.

Before further studies the carbonizates (D–Na and D–Ca) obtained in this way were washed (in the extraction column) with 6% hydrochloric acid, then with distilled water in order to remove mineral parts from them and afterwards they were dried.

Activation of carbonizates

Activation of D–Na, D–H and D–Ca samples (not washed with hydrochloric acid) with water vapour was carried out in the fluidal reactor. Water was added to the reactor through the evaporator (350°C) with a rate 0.6 mL min^{-1} by means of peristaltic pump (Cole Palmer Instrument Company, USA). The carbon material sample was heated in the reactor to 800°C in the deoxidized nitrogen stream (300 mL min^{-1}), then the nitrogen flow was cut off and water vapour was added into the reactor for 0.5 h. After this period of time the water flow was stopped and the sample was cooled in the nitrogen stream. Before further studies the activated samples were washed with hydrochloric acid in the way described above. They were designated with the symbols D–Na–ac, D–H–ac and D–Ca–ac.

Characterisation of materials

To study the textural characteristics of the materials, low-temperature (77.4 K) nitrogen adsorption–desorption isotherms were recorded using a Micromeritics ASAP 2405N (Norcross GA, USA) adsorption analyser. The specific surface area (S_{BET}) was calculated according to the standard BET method [20, 21]. The total pore volume V_p was evaluated by converting the volume of nitrogen adsorbed at $p/p_s \approx 0.95$ (p and p_s denote the equilibrium pressure and the saturation pressure of nitrogen at 77.4 K, respectively) to the volume of liquid nitrogen per gram of the material. The micropore volume (V_{mic}) was determined using the *t*-plot method [22], and mean pore radii $R_m=2V_p/S_{BET}$ were calculated from the adsorption data. The mesopore volume (V_{BJH}) was determined on the basis of Barrett–Joyner–Halenda (BJH) [23] theory on the basis of nitrogen adsorption data.

The pore size distributions (PSD) were calculated as differential functions $f_V(x)$ using the overall isotherm equation based on the combination of the modified Kelvin equation and the statistical adsorbed film thickness [24] applied to a model of slit-like pores of activated carbons. The desorption data (as the overall isotherms) were used to compute the $f_V(x)$ distributions with a modified regularization/singular value decomposition procedure Contin [25] under non-negativity constrains for $f_V(x)$ (i.e., $f_V(x) \geq 0$ at any x) at a fixed regularization parameter $\alpha=0.01$ [26]. For pictorial presentation the pore size distribution functions were calculated as incremental PSDs (IPSDs)

$$f_{z,n}(x_i)=0.5[f_z(x_i)+f_z(x_{i-1})](x_i-x_{i-1})$$

where subscript $z=V$ [27, 28].

Morphology of the materials was studied using a TESLA BS 301 scanning microscope. Atomic forces microscope (AFM) images were obtained by means of a Nanoscope III (Digital Instruments, USA) apparatus using a Tapping Mode AFM measurements technique.

Results and discussion

The results of thermal analysis in argon atmosphere (TG, DTG and DTA) of the studied samples are shown in Fig. 1. Table 1 includes quantitative data obtained from the analysis of these curves. For comparison the literature data [8] are put into table.

As can be seen (curves TG and DTG) about a temperature 400°C a rapid drop of the D–Na sample mass accompanied by a distinct exothermic effect (DTA peak maximum at 420°C) is observed. It proved unexpectedly that this effect is due to 'jumping out' of resin grains from the derivatograph crucible. Therefore there was changed the temperature program of sample heating, i.e. about this temperature (400°C) there was changed the rate temperature increment to 1°C min^{-1} but at lower and higher temperatures 5°C min^{-1} were maintained. Also in this case 'jumping out' of grains from the crucible was not avoided.

The thermal analysis of hydrogen (D–H) and calcium (D–Ca) forms of Duolite C20 took a quite different course. Comparing the corresponding curves in Fig. 1 one can see that both pyrolized forms of the ion exchanger have the extrema on both DTA and DTG curves at similar temperatures. For the hydrogen form (D–H) the endothermic effects (minima on the DTA curves) occur close to temperatures 129, 298 and 469°C (weak effect). However, for the calcium form (D–Ca) these minima are observed at 125, 303 and 480°C (Fig. 1). Endothermic effect at the lowest temperatures (138, 125 and 129°C for the sodium, calcium and hydrogen form, respectively) can result from dehydration of the studied samples. For the hydrogen form (D–H) there is observed a deepest minimum on the DTA curve at 129°C (for sample from [8] it was about 143°C) which can be due to larger affinity of the sample surface for water than that of the D–Ca sample. Next minima connected with endothermic effects at temperatures to about 290°C, according to the authors of [5, 9] can result from depolymerization of the polystyrene-divinylbenzene structures of the resins which is connected with desulfonation. At higher temperatures degradation of polystyrene and divinylbenzene structure takes place [8]. Comparing the corresponding data (Table 1) for two hydrogen forms of studied resin and resin from literature [8] it can be noticed the differences in total TG mass losses (74.6% for sample D–H and 43.3% for sample [8]). However similar TG mass losses in the temperature ranges of 200–400°C and especially 280–320°C in which the sharp mass losses are observed. These differences probably are the results of different originate of these resins as well as the experiment conditions. In cited paper [8] the conditions of thermal treatment during TG–DTG–DTA experiments were 10°C min^{-1} in the nitrogen atmosphere (in our experiments it was 5°C min^{-1} in argon). The used ion-exchanger was manufactured by Rohm and Haas and this resin was in a uniform fine powder (about 50 μm). These data could affect on differences both in characteristic DTA temperatures of thermal decompositions and TG mass losses in chosen temperature ranges.

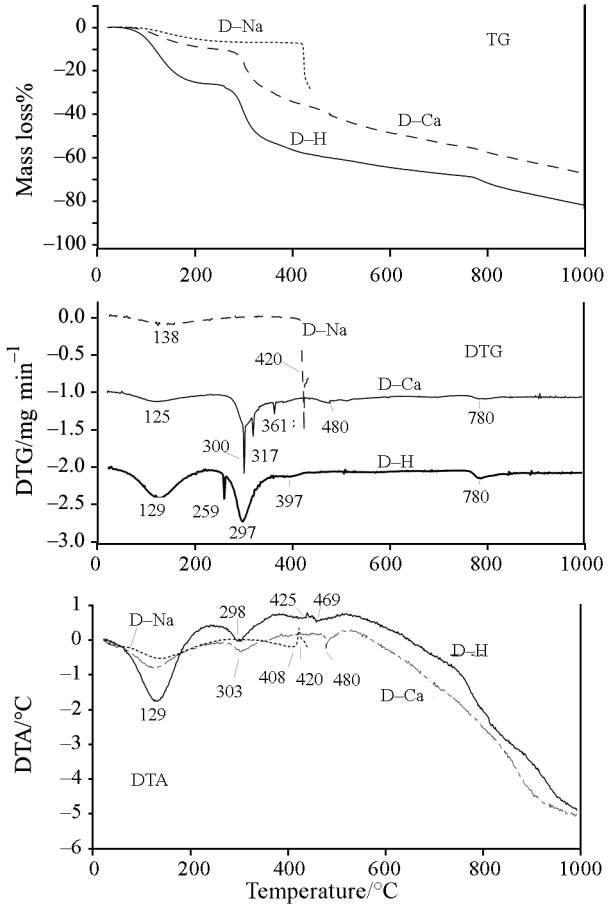

Fig. 1 TG, DTG and DTA curves of sodium, hydrogen and calcium forms (D–Na, D–H and D–Ca) of Duolite C20 heated with the temperature increment rate 5°C min^{-1}

Thermal destruction of thermoreactive cross-linked polymers can be considered as the process of structure ordering accompanied by condensation of benzene rings (nuclei) and formation of complex polycyclic ring-system macromolecules. These reactions proceed through decomposition and release of functional groups [29]. Defects in structures of hexagonal planes of carbon structural basic elements constitute pores of molecular sizes.

As follows from the analysis of curves in Fig. 1, the course of the above processes depends on temperature of pyrolysis and kind of the cation bonded with the functional surface group. As known [29] the higher pyrolysis temperature is, the better ordering of carbonizate structure takes place. As follows from Fig. 1, the sodium form of Duolite C20 exhibits large thermostability at about 400°C. In the other forms (D–H and D–Ca) of this

Table 1 TG mass losses of three forms of Duolite C-20 at different temperature ranges

Ion exchanger	TG mass losses/mass/mass%									
	25–200°C	200–400°C		280–320°C		400–800°C		800–1000°C		Total	
			*for dry sample		*for dry sample		*for dry sample		*for dry sample		*for dry sample
D–Na	5.1	1.9		0.2	0.22	21.1	22.2			28.1	
D–H	25.0	30.0	40.0	16.0	21.0	15.0	20.0	11.6	15.5	81.6	74.6
D–Ca	8.5	25.0	27.0	12.0	13.1	23.0	25.0	10.0	11.0	66.0	62.8
Duolite C20 H^+ [8]	33.0	23.0	34.0	14.0	21.9	6.0	9.0	0	0	62.0	43.3

*TG mass losses recalculated after subtracting of moisture at 200°C

resin, processes of depolymerization start much earlier which is accompanied by large mass losses. In the temperature range 200–400°C they are 40 and 27 mass/mass% for the hydrogen and calcium forms respectively (Table 1). Calcium, similar to sodium, increases thermal strength of the pyrolyzed resin compared to the hydrogen form. They also affect kinetics of depolymerization and functional group release in a given resin. This is evidenced by small differences in the values of corresponding temperatures in the DTG curve minima (Fig. 1) in which the rate of a given process is the largest and also by mass losses close to these temperatures (Table 1, interval 280–320 and 400–800°C).

From a practical and economical point of view it is essential that pyrolysis yield is the largest as far as products are concerned. The last column in Table 1 includes total losses of the pyrolyzed sample mass after taking off the adsorbed moisture mass. As follows a larger part of the sample mass is lost during pyrolysis.

In the above experiments the carbonizates of poorly (D–Na, Fig. 2) or well preserved (D–H, D–Ca, Fig. 3) spherical shapes are obtained. As can be seen in photos concavities and cracks occur on the surface of all carbonizates. However, as expected the specific surface area and volume of the pores of these samples

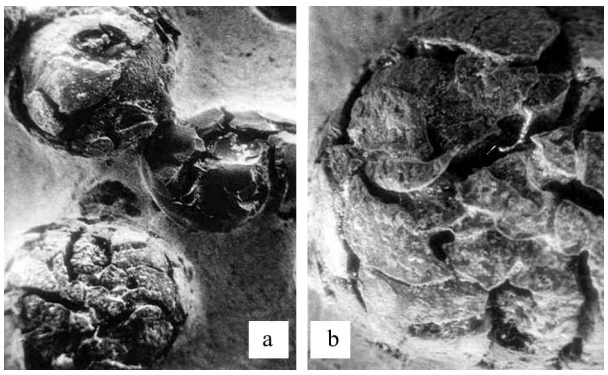

Fig. 2 SEM images of carbonizate of sodium form (D–Na) of Duolite C20 (magnifications: a – ×170, b – ×370)

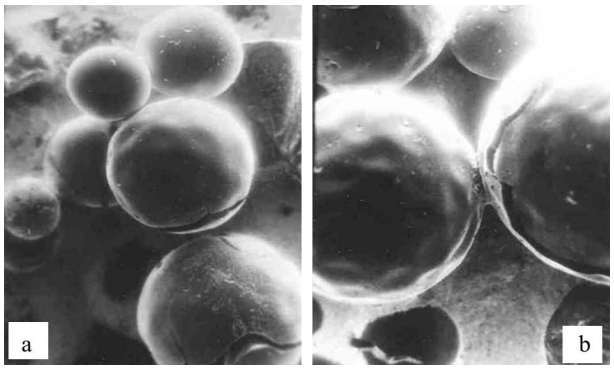

Fig. 3 SEM images of carbonizates of a – hydrogen and b – calcium forms of Duolite C20 (magnifications: a – ×200, b – ×190)

are very small (on the level of measuring error) which is in agreement with the results of studies similar polymers [5]. It is essential that mechanical strength of the obtained carbonizates is high. Richer facture of the D–Na sample results from a large content of sodium compounds.

Activation

Figure 4 shows the isotherms of nitrogen adsorption/desorption on the carbonizate samples which were activated with water vapour. As can be seen these isotherms are typical for microporous materials. The hysteresis loops for the adsorbents D–Na–ac, D–H–ac and D–Ca–ac can be attributed to type H4 (sodium and hydrogen forms) and H3 (calcium form) according to the IUPAC classification [30, 31]. As a result of Duolite C20 sodium form activation, the material characterized by a much worse formed hysteresis loop is obtained. H3 type is characteristic for the adsorbents possessing mostly slit-like pores but H4 type for the systems consisting of flat-parallel molecules [29]. In the case of two adsorbents, the hysteresis loops exist practically in the whole range of pressures p/p_s. This indicates that there are the system of complicated shape (probably bottle-shape) pores therefore nitrogen desorption from such pores is slow (delayed). This may be the result of too short activation time (small burst) as shown by the values of structural parameters of the carbon adsorbents (Table 2). The specific surface areas (S_{BET}) are not large compared with typical active carbons. However, carbon adsorbents of very wide of S_{BET} values are used in practice [32–34].

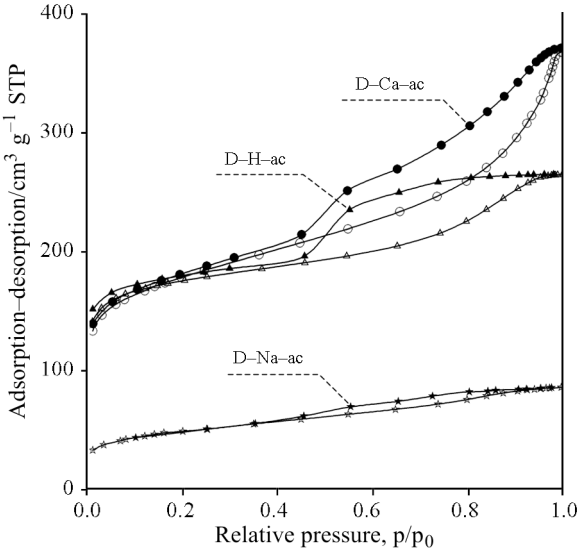

Fig. 4 Low-temperature adsorption-desorption isotherms of nitrogen for active carbons (D–Na–ac, D–H–ac and D–Ca–ac) prepared on the basis of sodium, hydrogen and calcium forms of Duolite C20

Table 2 Structural characteristics of active carbons prepared on the basis of three forms of Duolite C-20

Adsorbent	S_{BET}/m^2 g^{-1}	V_{por}/cm^3 g^{-1}	V_{mic}/cm^3 g^{-1}	V_{mic}/V_{por}	V_{BJH}/cm^3 g^{-1}	R_m/nm
D–Na–ac	173	0.13	0.02	0.15	0.10	1.5
D–H–ac	614	0.41	0.18	0.44	0.22	1.3
D–Ca–ac	629	0.56	0.13	0.23	0.43	1.8

As follows from the data in Table 2, parameters of porous structure of the prepared carbon adsorbents depend on the kind of cation embedded on the carbonized resin. The most microporous adsorbent is prepared by carbonization and activation of hydrogen form (compare the quantities V_{mic}/V_{por}, Table 2). The calcium form allows obtain carbons of the largest value S_{BET}, relatively large pore volume V_p, and volume of mesopores V_{BJH}. These observations are well reflected on Fig. 5 where incremental pore size distributions are presented. The PSDs for these samples show distinct contribution of micropores (x<1.1 nm) and narrow mesopores (x<1.3 nm) for all studied samples but significant ones are observed for D–H–ac and D–Ca–ac. Moreover carbon D–Ca–ac is characterized by marked contribution of mesopores up to x<40 nm.

Figure 6 includes the exemplary AFM photos of the D–H sample. Even with significant enlargement (220000 times, Fig. 6b) not very differentiated surface facture was obtained. Therefore this sample is nonporous as also confirmed by the specific surface area measurements.

However, the characteristic feature of this sample is the presence of fine grains of 30 to 100 nm sizes, set into gathered and compact structure of its surface. It should be mentioned again that these grains were not visible in the SEM picture (Fig. 3) of much smaller magnification. It can be supposed that these are condensed liquid products of resin decomposition which got out of its particles interior during pyrolysis.

Activation with water vapour of the D–H sample in question at 800°C allowed to prepare synthetic active carbon D–H–ac whose particles possess quite different surface facture compared with the initial carbonizate. Much spectacular information is provided in Fig. 7 in which long transport canals of various width (to 400 nm), present among carbon particle aggregates arranged in the chain form, can be distinctly seen which indicates that in this case the chain structure of the initial ion exchange resin is preserved. During the activation process additional fine grains observed before in Fig. 6 were removed.

Much information about the structure quality of the D–H–ac sample is given in Fig. 8 where carbon aggregates (about 300 nm) built of a large number of smaller (from 15 nm) and larger (to 60 nm) carbon particles can be seen.

While discussing the D–H–ac sample surface character, the fact that carbon particle aggregates are larger and more compact in some places should be pointed that is illustrated in Fig. 9. Quite homogeneous surface structure, much less spatially developed than the surface in Fig. 8 as well as much smaller slits present between aggregates can be seen here.

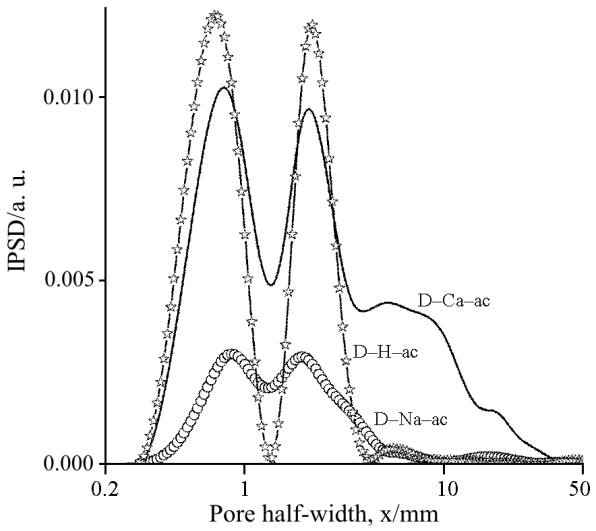

Fig. 5 Incremental pore size distributions with respect to pore volume of activated carbons (D–Na–ac, D–H–ac and D–Ca–ac) prepared on the basis of sodium, hydrogen and calcium forms of Duolite C20

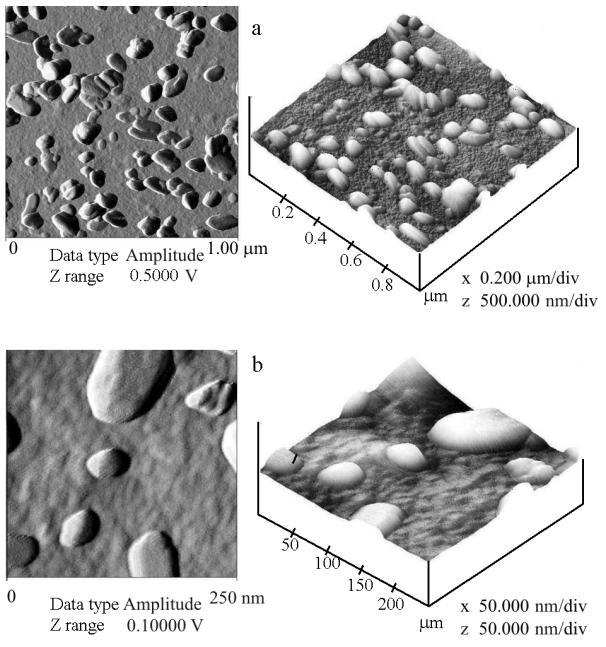

Fig. 6 2D and 3D AFM images (a – 1×1 µm, b – 250×250 nm) of D–H sample

Table 3 Structural heterogeneity parameters calculated for samples D–H and D–H–ac

Sample	Max. height, R_{max}/nm	Project surface area/nm^2	Surface area/nm^2	Surface area diff./%	Mean roughness, R_a/nm
D–H (Fig. 6)	56	250000	280440	12.2	4.482
D–H–ac (Fig. 8)	199	250000	367062	46.8	19.729
D–H–ac (Fig. 9)	19	250000	273047	9.2	1.728

Max. height (R_{max}) – maximum vertical distance between the highest and lowest data points within the cursor box; surface area – the three-dimensional area of the region enclosed by the cursor box. This value is the sum of the area of all the triangles formed by the three adjacent data points; surface area diff. – the percentage of the difference between the analyzed region's three-dimensional surface area and its two-dimensional project surface area; mean roughness (R_a) – arithmetic average of the absolute values of the surface height deviations measured from the mean plane within the box cursor: $R_a = \frac{1}{n}\sum_{j=1}^{n}\left|Z_j\right|$

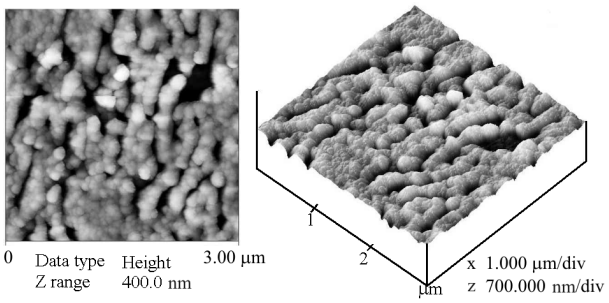

Fig. 7 2D and 3D AFM images (3×3 μm) of D–H–ac sample

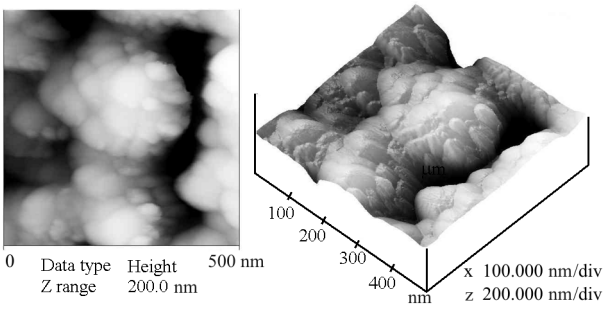

Fig. 8 2D and 3D AFM images (500×500 nm) of D–H–ac sample (example 1)

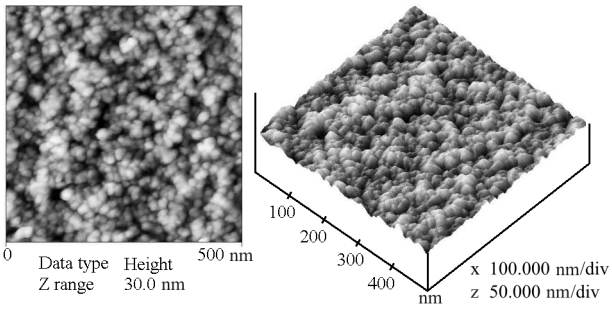

Fig. 9 2D and 3D AFM images (500×500 nm) of D–H–ac sample (example 2)

To compare the differences between the character of D–H carbonizate sample surface and that of D–H–ac active carbon, the parameters determining their structural heterogeneity proposed in [35] were used. These parameters were calculated for AFM pictures of 500 nm side. For D–H-ac sample these are Figs 8 and 9 and for D–H sample a fragment of the picture (500×500 nm) presented in Fig. 6a. The obtained data are given in Table 3. The data in Table 3 confirm the conclusions about differences in structural heterogeneity of the studied carbon samples. As can be seen the active carbon D–H–ac surface in Fig. 8 is the most spatially developed as indicated by the highest values of calculated parameters. Though the comparison of the data D–H (Fig. 6) and D–H–ac (Fig. 9) samples show that the carbonizate sample is sufficiently well spatially developed. These structural heterogeneities are due only to presence of additional grains on its surface.

Conclusions

The use of different forms of the sulfonated ion exchange resin Duolite C20 allows to prepare synthetic active carbons of spherical shape and different porous structure parameters. The specific surface areas S_{BET} achieved were 614 and 629 m^2 g^{-1} for active carbons prepared on the basis of hydrogen and calcium forms of resin respectively. Active carbon from hydrogen form of resin possessed more microporous structure. After carbonization and steam activation processes there was preserved the chain structure of initial polymer structure.

Acknowledgements

R. L. is grateful to the Foundation for Polish Science for financial support. The authors thank Prof. V. M. Gun'ko for the pore size distributions (PSDs) calculations.

References

1 N. T. Kartel, A. M. Puziy and V. V. Strelko, in: Characterisation of Porous Solids, Elsevier Science Publisher, Amsterdam 1991.
2 V. P. Musakina and T. G. Plachenov, Zhurn. Prikl. Khimii (Russian), 12 (1969) 2756.

3 K. Miura, J. Hayashi and K. Hasimoto, Carbon, 30 (1992) 946.
4 H. Teng and S. C. Wang, Carbon, 38 (2000) 17.
5 K. Bratek, W. Bratek and M. Kułażyński, Carbon, 40 (2002) 2213.
6 W. Grzegorczyk, J. Skubiszewska-Zięba and R. Leboda, The recycling of ion-exchange resin for carbon sorbents, In: Abstract of 3rd Congress of Chemical Technology, Gliwice, Poland 2000, p. 185.
7 A. Gierak, Mater. Chem. Phys., 41 (1995) 128.
8 M. A. Dubois, J. F. Dozol, C. Nicotra, J. Serose and C. Massiani, J. Anal. Appl. Pyrolysis, 31 (1995) 129.
9 T. Kyotani, Carbon, 38 (2000) 269.
10 K. László, A. Bóta, L.-G. Nagy and I. Cabasso, Colloids Surf., A 151 (1999) 311.
11 S. Villar-Rodil, A. Martinez-Alonzo and J. M. Tascón, J. Therm. Anal. Cal., 79 (2005) 529.
12 J. M. Salla, J. M. Morancho, X. Ramis and A. Cadenato, J. Therm. Anal. Cal., 80 (2005) 163.
13 T. Kojima, M. Tsuchija, K. Ishimaru and T. Yamada, J. Therm. Anal. Cal., 80 (2005) 137.
14 L. Degirmenci and T. Dumsoy, J. Therm. Anal. Cal., 79 (2005) 663.
15 A. F. Naves, P. M. Kosaka, J. R. Matos and D. F. S. Petri, J. Therm. Anal. Cal., 79 (2005) 389.
16 V. Vargha and Gy. Kiss, J. Therm. Anal. Cal., 76 (2004) 295.
17 S. M. Dakka, J. Therm. Anal. Cal., 75 (2004) 765.
18 R. Leboda, J. Skubiszewska-Zięba and V. I. Bogillo, Langmuir, 12 (1997) 1211.
19 R. Leboda, J. Skubiszewska-Zięba and W. Grzegorczyk, Carbon, 36 (1998) 417.
20 S. J. Gregg and K. S. W. Sing, Adsorption, Surface Area and Porosity, Academic Press, London 1982.
21 A. W. Adamson and A. P. Gast, Physical Chemistry of Surface, Wiley, New York 1997.
22 B. C. Lippens and J. H. de Boer, J. Catal., 4 (1965) 319.
23 E. P. Barrett, L. G. Joyner and P. P. Halenda, J. Am. Chem. Soc., 73 (1951) 373.
24 C. Nguyen and D. D. Do, Langmuir, 15 (1999) 3608.
25 S. W. Provencher, Comp. Phys. Comm., 27 (1982) 213.
26 V. M. Gun'ko and D. D. Do, Colloids Surf., A 193 (2001) 71.
27 V. M. Gun'ko and S. V. Mikhalovsky, Carbon, 42 (2004) 843.
28 V. M. Gun'ko, V. V. Turov, J. Skubiszewska-Zięba, B. Charmas and R. Leboda, Adsorption, 10 (2004) 5.
29 V. B. Fenelonov, Porous Carbon, Novosibirsk 1995.
30 K. S. W. Sing, D. H. Everett, R. A. W. Haul, L. Moscou, R. A. Pierotti, J. Roquerol and T. Siemieniewska, Pure Appl. Chem., 57 (1985) 603.
31 J. Roquerol, D. Avnir, C. W. Fairbridge, D. H. Everett, J. H. Hayness, N. Pernicone, J. D. F. Ramsay, K. S. W. Sing and K. K. Unger, Pure Appl. Chem., 66 (1994) 1739.
32 R. Leboda, Mater. Chem. Phys., 31 (1992) 243.
33 R. Leboda, Mater. Chem. Phys., 34 (1993) 123.
34 E. Matisova and E. Skrabakova, J. Chromatogr., 707 (1995) 145.
35 NanoScope Command Reference Manual Version 5. 12.

Received: July 1, 2005
Accepted: July 27, 2005
OnlineFirst: May 29, 2006

DOI: 10.1007/s10973-005-7150-5